BABEŞ-BOLYAI UNIVERSITY
FACULTY OF PHYSICS
DOCTORAL SCHOOL OF PHYSICS

PHD THESIS SUMMARY

Physical Properties of Low-Dimensional Systems: A Theoretical Study on Quantum Dots, Nanowires and Graphene

Levente MÁTHÉ

Scientific Supervisor

Prof. dr. Ioan GROSU

Cluj-Napoca
2023

Abstract

The main goal of the thesis is to theoretically investigate the quantum transport processes present in quantum dot-based nanodevices and to study the optical properties of spherical quantum dots. The first Chapter of the thesis is an introductory section which focuses on a brief discussion of basic concepts related to the topics. The second Chapter of the thesis proposes an experimentally feasible nanojunction in which a quantum dot is integrated in a semiconducting-superconducting heterostructure hosting Majorana bound states in the presence of an optical phonon mode. A threading magnetic flux is used to manipulate the Majorana-induced phonon-assisted quantum tunneling. Our findings can serve as a promising guide in Majorana detection experiments. The next Chapter of the thesis focuses on a detailed theoretical study of quantum transport in a setup consisting of two graphene electrodes between which a quantum dot is interposed under the effect of the magnetic field. The proposed system can provide an ideal platform for the investigation of many-body quantum phenomena, such as the Kondo effect, and can be regarded as a reference for the development of graphene-based nanoelectronic devices. The last part of the thesis focuses on the theoretical study of linear and nonlinear optical properties of a spherical semiconductor quantum dot in which the quantum confinement is due to an inversely quadratic Hellmann potential within the effective mass approximation. The proposed setup could be further utilized to boost the development of novel quantum dot-based optoelectronic devices.

Keywords: *quantum transport, quantum dots, Majorana bound states, electron-phonon interaction, optical phonons, graphene, Kondo effect, absorption coefficient, refractive index changes.*

Contents of the Thesis

Contents of the Summary

Chapter 1

Theoretical Background

1.1 Introduction to Low-Dimensional Systems. Quantum Dots and Kondo Effect

In the development of electronic components, it is necessary to take into account the quantum phenomena occurring in nanoscale devices and to study them theoretically. A system is nanoscale if the characteristic size of the transport region is smaller than the electron phase-coherence length but it is comparable with the de Broglie wavelength of the electron and exhibits discrete energy spectrum [1, 2]. Quantum dots (QDs) are small confined regions of dimensions comparable with the electron de Broglie wavelength, considered as zero-dimensional objects, are embedded between semi-infinite electrodes which play the role of electron reservoirs as it is shown in Figure 1.1(a). The dot tunnel couples to the left (right) lead with coupling $\Gamma_{L(R)}$. The motion of electrons is restricted in all spatial directions, and thus they occupy discrete energy levels in the QD, which can be probed in transport measurements via macroscopic electrodes. The confinement induced energy levels can be controlled via changing the potential characteristics. The total QD spectrum is a result of the confinement induced and the charge quantization generated energy spectrum [3]. Figure 1.1(b) illustrates an experimental realization of a QD fabricated in GaAs semiconductor heterostructure [5].

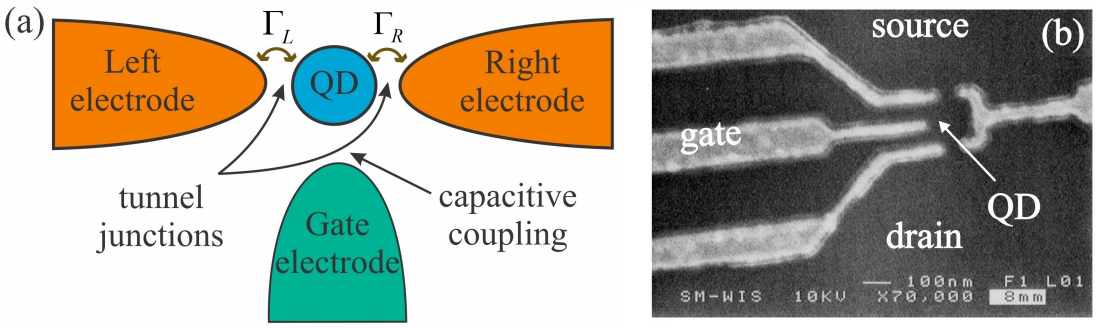

Figure 1.1: Schematic representation of a quantum dot (QD) coupled to left and right electrodes via tunnel junctions with couplings Γ_L and Γ_R, respectively. The gate electrode is capacitively attached to the QD. Figure based on [3, 4]. (b) Scanning Electron Microscopy image of a QD [5].

As known, the electrical resistance of metals (e.g., Cu, Au) decreases when the temperature is lowered and further decrease in temperature leads to the saturation of resistivity [6, 7]. A group of metals (e.g., Al, Nb) may abruptly lose all their electrical resistance at a critical temperature when undergoing a phase transition from the conducting to a superconducting state. It has been observed that when magnetic atoms (e.g., Mn, Cr) are added to nonmagnetic metals, the electrical resistance starts to increase as the temperature further decreases, without exhibiting a phase transition. The temperature at which the electrical resistivity begins to grow again is called the Kondo temperature. The effect was first explained by Kondo, considering antiferromagnetic coupling between magnetic impurities and a sea of conduction electrons [8]. Antiferromagnetic exchange between the spin of leads' electrons and the QD spin is realized by a second-order spin-flip cotunneling process for which the initial and final states of QD have different spin orientations. This results in opening of an additional transport channel at the Fermi energy by forming a resonance [9]. The peak emerging at the Fermi level in the density of states is called Kondo resonance. Contrary to bulk metals where the Kondo effect emerges as a $\ln T$ divergence of the resistivity [Figure 1.2(a)], in QDs it shows up as a $\ln T$ dependence of the linear conductance [Figure 1.2(b)]. The Kondo effect was first experimentally demonstrated in GaAs-based QDs [5, 10, 11].

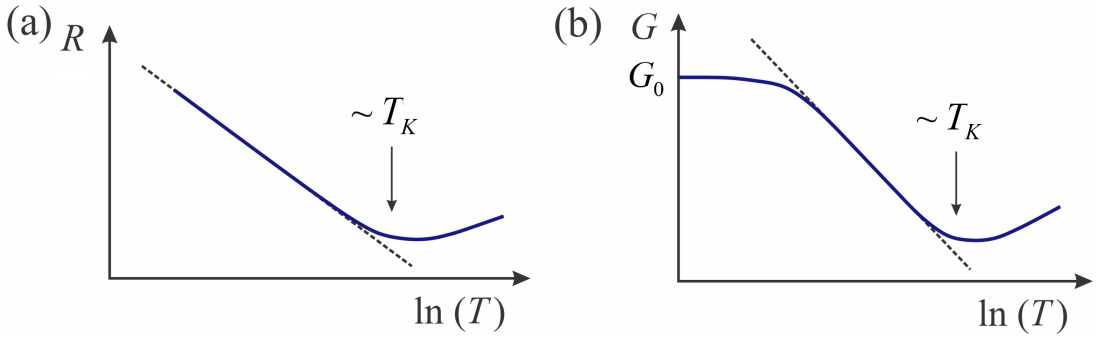

Figure 1.2: (a) The logarithmic dependence of resistivity R on temperature T in bulk metals. (b) The logarithmic dependence of conductance G on temperature T in QDs where $G_0 = 2e^2/h$ is the conductance quantum. Figures adapted from [9].

1.2 Introduction to the Majorana Fermions and Majorana Bound States

Majorana recognized in 1937 that the Dirac equation can be represented in terms of real wavefunctions [12] which entails an important consequence, a particle described by a real wavefunction is its own antiparticle. The particles that fulfill this condition are charge-neutral, called Majorana fermions (MFs). Due to the fact that the Majorana equation has the same mathematical structure as the Bogoliubov-de Gennes equation which describes the quasiparticle excitations in superconductors (SCs), thus MFs can be searched in SCs. MFs in SCs are midgap excitations with zero-energy ($E = 0$) for spinless fermions, called Majorana zero modes (MZMs) or equivalently Majorana bound states (MBSs). The MFs in condensed matter can be created as zero-energy excitations in spinless or p-wave SCs with spin-triplet pairing [13, 14]. The fingerprints of MBSs were first seen in transport measurements in such heterostructures as a zero-bias anomaly in differential conductance map [15]. We briefly discuss two models which allow to create MBSs in topological SCs: the Kitaev model [16] and the Oreg-Lutchyn model [17, 18].

The Kitaev model [16] involves spinless electrons deposited on the surface of a p-wave superconducting lattice with N finite sites. Note that the same lattice site is occupied by one spinless electron due to the Pauli exclusion. Due to the fact that any complex fermion can be split into two MFs, thus the chain of N complex fermions can be represented in terms of $2N$ MFs. When the coupling between MFs localized on neighboring lattice sites is stronger than the coupling strength between the Majoranas from the same lattice sites, the first and last MFs are decoupled from the chain of $2N$ MFs. These two unpaired MFs are completely localized at the edges of the lattice and correspond to a single fermion mode which is delocalized between the two ends of the chain. These Majorana end modes are the Majorana bound states (MBSs). This phase is called topologically nontrivial [19].

Since p-wave SCs with spin-triplet pairing form the category of unconventional SCs, they appear rarely in the nature and thus they should be replaced by other realizations in experiments [19, 20]. It has been established that a possible experimental realization of the Kitaev one-dimensional lattice chain model is obtained when depositing a semiconducting nanowire with strong spin-orbit coupling (eg., InAs, InSb), as shown in Figure 1.3, in proximity of a con-

ventional s-wave SC (eg., Al, Nb) in an external magnetic field [17, 18]. The proposed system is called Oreg-Lutchyn model. When the relation $h > \sqrt{|\Delta|^2 + \mu^2}$ between Zeeman energy (h), the proximity induced superconducting gap (Δ) and chemical potential of nanowire (μ) is fulfilled, the system can be mapped into the Kitaev model by hosting at its ends MBSs [21]. In this case the semiconductor nanowire is transformed into a topological superconducting nanowire (TSNW), a setup usually called in literature Majorana nanowire [19]. In a finite system with size L, the two Majorana wavefunctions overlap leading to a hybridization of MZMs characterized by the overlap energy $\varepsilon_M \propto e^{-L/\xi}$ where ξ is the superconducting coherence length [19].

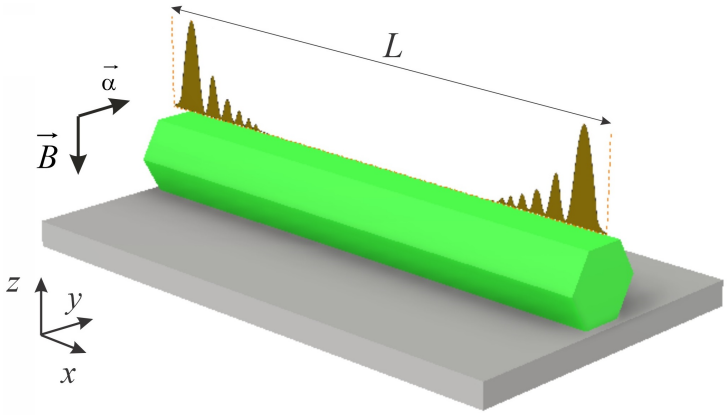

Figure 1.3: A TSNW as a result of a proximity of a semiconducting nanowire with strong spin-orbit coupling of strength α (represented in green) with an s-wave superconductor (represented in gray) in the presence of a magnetic field ($\vec{B}$). The Majorana modes appear at the opposite ends of the TSNW (represented in orange) that overlap for a finite L length nanowire. Figure adapted from [13, 14, 19, 21].

The MBSs appear as a pair of spatially separated localized edge modes in topological SCs which can store information as a nonlocal regular fermionic state. The existence of MBSs is not influenced by local perturbations and, in general, they are protected from quantum decoherence.

1.3 Graphene

Graphene is a two-dimensional crystal for which the sp^2 hybridized carbon atoms condense in a hexagonal lattice structure which can be viewed as a triangular lattice with two carbon atoms per unit cell [22]. The graphene as monolayer graphite was first theoretically predicted more than a half century ago [23] and isolated experimentally for almost two decades [24]. Graphene owns high electron mobility, good thermal conductivity, unique mechanical and opti-

cal properties [25] which makes it a suitable platform for many applications such as fabrication of electronic sensors [26], optoelectronic [27] or energy storage devices [28]. The reciprocal lattice of monolayer graphene contains high symmetry crystallographic points, K and K', located at the corners of the first Brillouin zone, which, are also called Dirac points.

The band structure of graphene can be determined within a tight-binding approximation and near the Dirac points the energy dispersion is $E_{\pm}(q) \approx \pm\hbar v_F|\vec{q}|$ with $v_F \approx 10^6$ m/s being the graphene Fermi velocity where the sign $+/-$ refers to the conduction/valance band. They touch each other at the Dirac points [22]. The energy dispersion of graphene at the Dirac points is linear in momentum [as seen in Figure 1.4(a)] presenting no energy gap [29]. The charge carriers in graphene are called massless Dirac fermions. For an undoped graphene, the Fermi level is located at the Dirac point where the electron and hole bands touch each other in the momentum space. The density of states (DOS) $\rho(E)$, near the Dirac points, is $\rho(E) = g_s g_v |E|/2\pi\hbar^2 v_F^2$ where $g_s = 2$ and $g_v = 2$ are the valley and spin degeneracy [30]. Figure 1.4(b) illustrates the DOS near the Dirac point and for a full bandwidth.

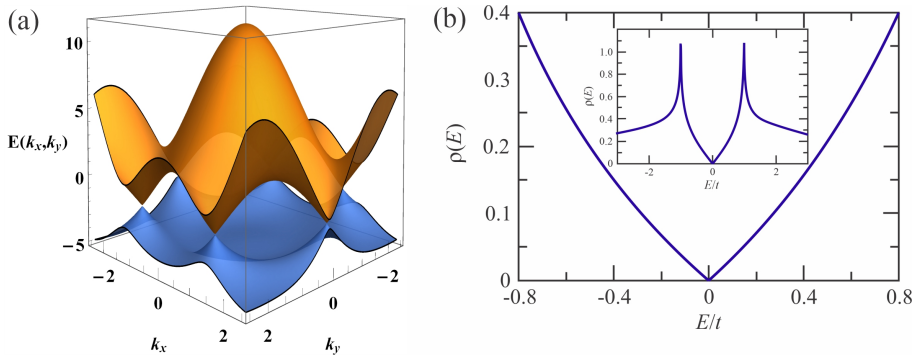

Figure 1.4: (a) Band structure $E(k_x, k_y)$ of graphene. (b) DOS $\rho(E)$ of a monolayer graphene near the Dirac point and over a full energy domain (inset). Figures adapted from [22, 29].

Chapter 2

Probing Majorana Bound States via Quantum Dots in the Presence of Electron-Phonon Interaction

2.1 Motivation

The discovery of Majorana bound states (MBSs) have opened a new research area in the condensed matter community. The most commonly employed scheme to probe MBSs in a topological superconducting nanowire (TSNW) consists of the coupling of MBSs to a quantum dot (QD), which is then coupled to normal leads [31, 32]. The signature of MBSs is seen in the linear conductance measured through the dot [32]. Namely, when a noninteracting QD connects to a nanowire which is in its topological superconducting phase, the presence of MBSs manifests in the reduction of linear conductance peak to $e^2/2h$. Over the last few years, various QD-TSNW structures have been theoretically proposed in order to detect the fingerprints of Majoranas via transport properties, such as conductance [33–35], thermal conductance [36, 37] and Fano resonance [38, 39]. Over the past decade, a plethora of experimental realizations on the detection of Majorana signatures via transport measurements have been reported by using devices based on normal lead-superconductor (SC) junctions [15, 40] or different QD-TSNW configurations [41, 42]. In particular, a couple of theoretical studies have addressed the phonon-assisted transport mechanisms at MZMs [43–47].

The aim of this Chapter is to propose a realistic, experimentally feasibly setup, that can probe MBSs via transport measurements. We show that the characteristic signatures expected from Majorana modes are significantly modified in the presence of electron-phonon interaction (EPI).

2.2 Theoretical Model

The system consists of a dot which is connected to two Majoranas hosted by the ends of a TSNW. The QD-TSNW configuration forms a loop structure that is threaded by an external

magnetic flux Φ, as it is illustrated in Figure 2.1. Thus, the transport properties of the nano-junction can be manipulated when tuning the magnetic flux. To investigate the effect of the EPI on transport properties, we consider that the localized electron in the dot interacts with a single long-wave optical phonon mode. The system is modeled by the Hamiltonian [32, 34, 38, 48]

$$\begin{aligned}\mathcal{H} = &\sum_{\alpha,k} \varepsilon_{\alpha k}\, c^{\dagger}_{\alpha k} c_{\alpha k} + i\varepsilon_M \gamma_1 \gamma_2 + \hbar\omega_0 a^{\dagger} a + \varepsilon_d d^{\dagger} d + \beta(a + a^{\dagger}) d^{\dagger} d \\ &+ \left[(\lambda_1 d - \lambda_1^{*} d^{\dagger})\gamma_1 + i(\lambda_2 d + \lambda_2^{*} d^{\dagger})\gamma_2\right] + \sum_{\alpha,k} \left(V_{\alpha k} c^{\dagger}_{\alpha k} d + V^{*}_{\alpha k} d^{\dagger} c_{\alpha k}\right).\end{aligned} \tag{2.1}$$

The first term of Eq. (2.1) describes the motion of free electrons in both electrodes where $c_{\alpha k}$ ($c^{\dagger}_{\alpha k}$) denotes the annihilation (creation) operator for a noninteracting electron with momentum k in the normal lead α [where $\alpha \equiv$ left (L), and right (R)] and μ_α denotes the chemical potential in lead α. The electrodes are at the same temperature, $T_\alpha = T$. The second term in Eq. (2.1) characterizes the coupling between the two Majoranas (denoted by γ_1 and γ_2), hosted by the opposite ends of the TSNW loop via ε_M Majorana overlap energy. The third term in Eq. (2.1), represents the longitudinal optical phonon mode with $a^{\dagger}(a)$ phonon creation (annihilation) operator and $\hbar\omega_0$ phonon energy. The phonon distribution is $N_{\text{ph}} = 1/(e^{\hbar\omega_0/k_B T} - 1)$ (in the following $\hbar = k_B = 1$). The fourth term in Eq. (2.1) describes the single-level QD where

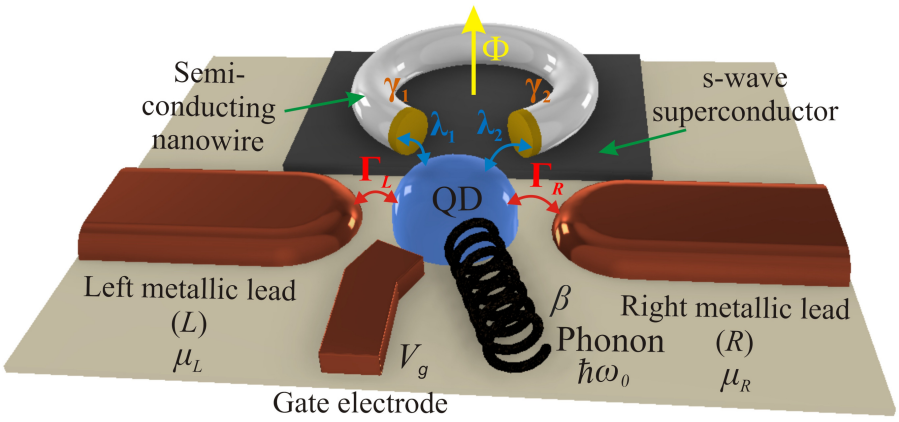

Figure 2.1: Schematic representation of a QD attached to two MBSs, denoted by Majorana operators γ_1 and γ_2, via coupling strengths λ_1 and λ_2, hosted by the ends of a TSNW. The QD-TSNW setup forms a loop structure which is threaded by a tunable magnetic flux Φ. The QD is connected to left (L) and right (R) metallic electrodes via coupling strengths Γ_L and Γ_R, respectively. The chemical potential in lead $L(R)$ is denoted by $\mu_{L(R)}$. The QD level is tuned by the gate voltage V_g applied to the gate electrode. The QD electron interacts with an optical phonon mode of frequency ω_0 via the electron-phonon coupling strength β.

ε_d is the dot energy and $d^\dagger(d)$ stands for the fermionic creation (annihilation) operator for dot electrons. The next term of Eq. (2.1) characterizes the interaction between the dot electron and optical phonon mode via electron-phonon coupling strength β. The next term in Eq. (2.1) models the coupling of the dot to the Majoranas via coupling strengths $\lambda_1 = |\lambda_1|e^{i\phi/4}$ and $\lambda_2 = |\lambda_2|e^{-i\phi/4}$ [38] where the magnetic flux phase is defined as $\phi = \pi\Phi/\Phi_0 = 2\arg(\lambda_1/\lambda_2)$ and $\Phi_0 = h/2e$ represents the magnetic flux quantum. The last term of Eq. (2.1) describes the coupling between the dot electron and free electrons in normal leads via tunneling amplitudes $V_{\alpha k}$. The Majorana operators γ_1 and γ_2 are replaced with regular fermion operators, $\gamma_1 = (f^\dagger + f)/\sqrt{2}$ and $\gamma_2 = i(f^\dagger - f)/\sqrt{2}$, respectively.

In the framework of nonequilibrium Green's function formalism, the current flowing from the α normal lead to the QD is given by the relation [49–51]:

$$I_\alpha = \frac{ie}{h}\int d\varepsilon \big\{\mathbf{\Gamma}_\alpha(\varepsilon)\big[\mathbf{f}_\alpha(\varepsilon)[\mathbf{G}_d^r(\varepsilon) - \mathbf{G}_d^a(\varepsilon)] + \mathbf{G}_d^<(\varepsilon)\big]\big\}_{11}, \tag{2.2}$$

where $\mathbf{G}_d^{r(a)}(\varepsilon)$, $\mathbf{G}_d^{<(>)}(\varepsilon)$, $\mathbf{\Gamma}_\alpha(\varepsilon)$ and $\mathbf{f}_\alpha(\varepsilon)$ are the retarded (advanced), lesser (greater) Green's function matrices of the dot, QD-lead coupling matrix and Fermi-Dirac distribution matrix for electrode α represented in the Nambu space. Note that the Kirchhoff's law $I_S + I_L + I_R = 0$ is fulfilled [51]. In the subgap regime, $|eV| < \Delta$, the current I_α can be further decomposed as $I_\alpha = I_\alpha^{ET} + I_\alpha^{LAR} + I_\alpha^{CAR}$ where I_α^{ET}, I_α^{LAR} and I_α^{CAR} are the currents generated in the electron tunneling (ET), local and crossed Andreev reflection (LAR and CAR) processes. The ET process manifests in the transmission of an electron from one electrode to the other one. The LAR process refers to the tunneling of one electron/hole from one electrode into the SC via one MZM after that it is reflected as a hole/electron in the same electrode. In a CAR process a pair of MZMs connects to two normal electrodes in which one electron/hole from one electrode tunnels into the superconducting material via one MZM and then it tunnels out as a hole/electron via the other MZM at the other electrode [52]. Assuming electron-hole symmetry in QD-lead couplings $\Gamma_\alpha^e = \Gamma_\alpha^h = \Gamma$ and $\mu_L = -\mu_R = eV/2$ with $\mu_S = 0$ in SC, the total current through the dot reads

$$I = \frac{ie}{2h}\Gamma\int d\varepsilon\,\big[f_L^e(\varepsilon) - f_R^e(\varepsilon)\big][\mathbf{G}_d^>(\varepsilon) - \mathbf{G}_d^<(\varepsilon)]_{11}. \tag{2.3}$$

To calculate $\mathbf{G}_d^{<(>)}(\varepsilon)$, we employed the canonical transformation which allows us to eliminate the electron-phonon coupling term in Hamiltonian given by Eq. (2.1). The application

of canonical transformation leads to a new transformed Hamiltonian, decoupled into a phonon and an electron part, and to renormalization of the QD energy, dot-leads and dot-MBSs couplings $\tilde{\varepsilon}_d = \varepsilon_d - g\omega_0$, $\tilde{\Gamma}_\alpha = \Gamma_\alpha e^{-g(2N_{\rm ph}+1)}$ and $\tilde{\lambda}_j = \lambda_j e^{-g(N_{\rm ph}+1/2)}$ with $g = (\beta/\omega_0)^2$. The greater and lesser Green's functions are expressed as $\mathbf{G}_d^{>}(\varepsilon) = \sum_{p=-\infty}^{\infty} \mathcal{L}_p \tilde{\mathbf{G}}_d^{>}(\varepsilon - p\omega_0)$ and $\mathbf{G}_d^{<}(\varepsilon) = \sum_{p=-\infty}^{\infty} \mathcal{L}_p \tilde{\mathbf{G}}_d^{<}(\varepsilon + p\omega_0)$ where $\mathcal{L}_p$ denotes the Franck-Condon factor [48]. To determine the dressed lesser (greater) Green's functions, $\tilde{\mathbf{G}}_d^{<(>)}$, we applied the Keldysh equation, $\tilde{\mathbf{G}}_d^{<(>)} = \tilde{\mathbf{G}}_d^r \tilde{\mathbf{\Sigma}}^{<(>)} \tilde{\mathbf{G}}_d^a$, where $\tilde{\mathbf{\Sigma}}^{<(>)}$ is dressed lesser (greater) self-energy. The elements of retarded Green's function matrix $\tilde{\mathbf{G}}_d^r$ have been determined by employing the equation of motion technique [53]. Knowing $\mathbf{G}_d^{<(>)}(\varepsilon)$, all the transport properties of QD can be explored. The detailed calculations can be found in our work [54].

2.3 Results and Discussion

In this Section, we present the main results for transport properties of the QD-MZMs system in both the absence and the presence of EPI within several experimentally relevant parameter regimes. The superconducting gap Δ in typical experimental setups is on the order of $250\,\mu\text{eV}$ for TSNWs [15]. The values of QD-leads Γ and QD-MBSs $|\lambda_j|$ couplings are on the order of a few μeV [33]. In calculation, we measured all energies in units of Γ. The electron-phonon coupling strength and phonon energy are chosen as $\beta = 2.5\,\Gamma$ and $\omega_0 = 5\,\Gamma$, respectively.

2.3.1 Results in absence of electron-phonon interaction

In this Section, we study the behavior of linear ($\mathcal{G}$) and differential (dI/dV) conductance when varying the system parameters in the absence of EPI. To understand the influence of biasing on the periodicity of dI/dV in magnetic flux phase ϕ, we introduce $\mu_L = qeV$ and $\mu_R = (q-1)eV$ with $\mu_L - \mu_R = eV$ and $0 \leq q \leq 1$. We show in Figures 2.2(a) and (b) the results for zero-temperature total differential conductance dI_L/dV against the magnetic flux phase ϕ for nonoverlapping ($\varepsilon_M = 0$) and overlapping ($\varepsilon_M \neq 0$) MBSs. Figure 2.2(c) illustrates the CAR component of the zero-temperature total differential conductance, dI_L^{CAR}/dV. The dot level is not tuned, $\varepsilon_d = 0$. We observe that dI_L/dV exhibits a 2π-periodic function in ϕ for $\varepsilon_M = 0$ and remains unchanged when altering the system biasing. When $\varepsilon_M \neq 0$, the periodicity of dI_L/dV can be 2π and 4π depending on how the QD biasing is chosen. The CAR processes contribution

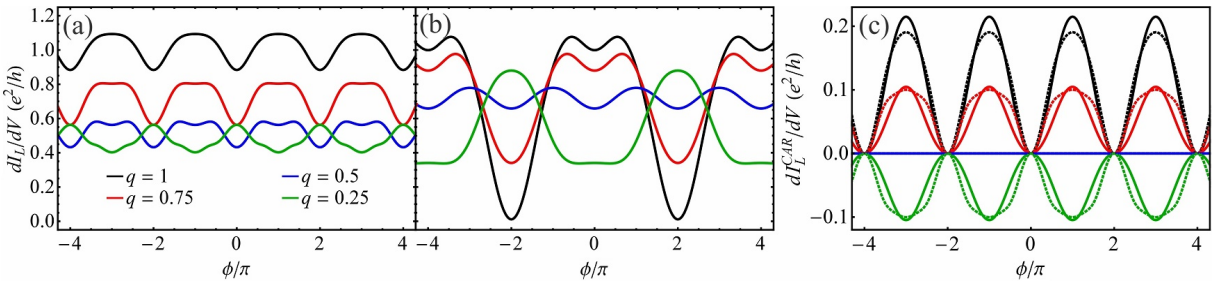

Figure 2.2: dI_L/dV versus ϕ with: (a) $\varepsilon_M = 0\,\Gamma$ and (b) $\varepsilon_M = 0.3\,\Gamma$. (c) dI_L^{CAR}/dV versus ϕ where the solid (dashed) lines correspond to $\varepsilon_M = 0.3\,\Gamma$ ($\varepsilon_M = 0\,\Gamma$). The QD is biased for different $\mu_L = qeV$ values with $eV = 0.28\,\Gamma$ and $\mu_L - \mu_R = eV$, $|\lambda_1| = |\lambda_2| = 0.3\,\Gamma_R$, $\varepsilon_d = 0\,\Gamma$ and $T = 0\,\Gamma$.

to dI_L/dV is finite except the case when $\mu_L = -\mu_R = eV/2$. Note that the periodicity of differential and linear conductances are not affected by a possible asymmetry arising in the dot-lead couplings ($\Gamma_L \neq \Gamma_R$). This further indicates that the conductance periodicity would be a robust signature in experiments.

In the following, we focus on the $\mu_L = -\mu_R = eV/2$ case when only the ET and LAR processes contribute to the linear and differential conductances. We explore the ET and LAR components of the zero-temperature linear conductance $\mathcal{G}$ when the coupling $|\lambda_2|$ is varied with fixed $|\lambda_1|$. The results are shown in Figure 2.3(a) for $\mathcal{G}$ with its ET ($\mathcal{G}_{ET}$) and LAR ($\mathcal{G}_{LAR}$) components versus magnetic flux phase ϕ for overlap energy $\varepsilon_M = 0$ when the QD energy is $\varepsilon_d = 0$. We observe that $\mathcal{G}_{ET}$ and $\mathcal{G}_{LAR}$ oscillate with a period of 2π with amplitudes $\mathcal{G}_{ET} = \mathcal{G}_{LAR} = e^2/4h$ and $\mathcal{G}$ reaches the $e^2/2h$ value, independent of the finite values of $|\lambda_2|$. Note that the zero-temperature linear conductances are independent of the values of dot energy ε_d. When $\varepsilon_M \neq 0$, $\mathcal{G}$ is composed from the ET conductance, $\mathcal{G} \approx \mathcal{G}_{ET}$, and it presents

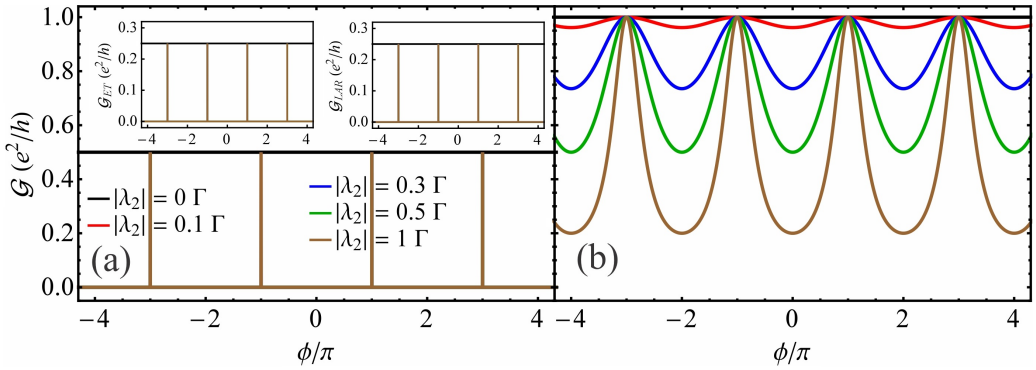

Figure 2.3: (a) $\mathcal{G}$ versus ϕ for $\varepsilon_M = 0\,\Gamma$. The left and right insets refer to the results for the ET ($\mathcal{G}_{ET}$) and LAR ($\mathcal{G}_{LAR}$) components of $\mathcal{G}$, as a function of ϕ. (b) $\mathcal{G}$ versus ϕ for $\varepsilon_M = 0.3\,\Gamma$. The coupling $|\lambda_1| = 0.3\,\Gamma$ is fixed and the coupling $|\lambda_2|$ is varied at $\varepsilon_d = 0\,\Gamma$ and $T = 0\,\Gamma$.

a 2π periodicity in ϕ at $\varepsilon_d = 0$ [see Figure 2.3(b)]. Contrary to the nonoverlapping Majoranas case, the maxima of $\mathcal{G}$ for hybridized MBSs reach the value e^2/h.

To further study the behavior of $\mathcal{G}$ in the regime $\varepsilon_d \neq 0$ and $\varepsilon_M \neq 0$, the zero-temperature total linear conductance $\mathcal{G} \approx \mathcal{G}_{ET}$ is plotted in Figure 2.4 as a function of magnetic flux phase ϕ and dot energy ε_d when the coupling strength $|\lambda_1|$ is fixed and the coupling $|\lambda_2|$ is varied. In the case of $\varepsilon_d = 0$, the linear conductance has a 2π periodicity as a function of ϕ. When the dot energy $\varepsilon_d \neq 0$, $\mathcal{G}$ exhibits a 4π periodicity in ϕ, independent of the finite values of QD-MBS coupling $|\lambda_2|$. Note that the differential conductance shows a 2π periodicity in magnetic flux phase ϕ for $\varepsilon_M = 0$ regardless the QD level ε_d tuning. For hybridized MBSs, the 2π periodicity of dI/dV in ϕ transforms to a 4π one when the dot energy ε_d is finite, $\varepsilon_d \neq 0$.

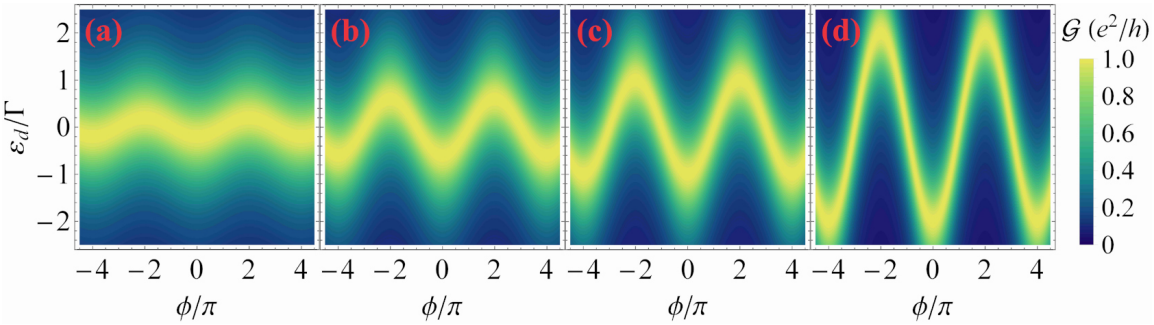

Figure 2.4: $\mathcal{G}$ versus ϕ and ε_d at $T = 0\,\Gamma$ with $\varepsilon_M = 0.3\,\Gamma$ and fixed coupling $|\lambda_1| = 0.3\,\Gamma$ at different $|\lambda_2|$ couplings: (a) $|\lambda_2| = 0.1\,\Gamma$, (b) $|\lambda_2| = 0.3\,\Gamma$, (c) $|\lambda_2| = 0.5\,\Gamma$ and (d) $|\lambda_2| = 1\,\Gamma$.

2.3.2 Results in presence of electron-phonon interaction

In this Section, we analyze the influence of EPI on the transport characteristics of the QD-MBS system. We plot in Figure 2.5 the linear conductance $\mathcal{G}$ versus magnetic flux phase ϕ at zero and a finite temperature for QD energy $\varepsilon_d = 0$, in the cases $\beta = 0$ and $\beta \neq 0$, for nonoverlapping and overlapping MBSs. We find that the zero-temperature linear conductance does not depend on the electron-phonon coupling strength β for nonoverlapping MBSs in agreement with the results for a QD attached to one MBS with EPI [45]. The linear conductance preserves its 2π periodicity in the presence of EPI for $\varepsilon_M = 0$. In the case of $\beta \neq 0$ with $\varepsilon_M \neq 0$, $\mathcal{G}$ depends on the QD level and β both at zero and nonzero temperatures. At $\varepsilon_M \neq 0$, the 2π periodicity of linear conductance as a function of ϕ changes to 4π under EPI which is attributed to the finite renormalized QD energy $\tilde{\varepsilon}_d$. Note that that the influence of the EPI on linear con-

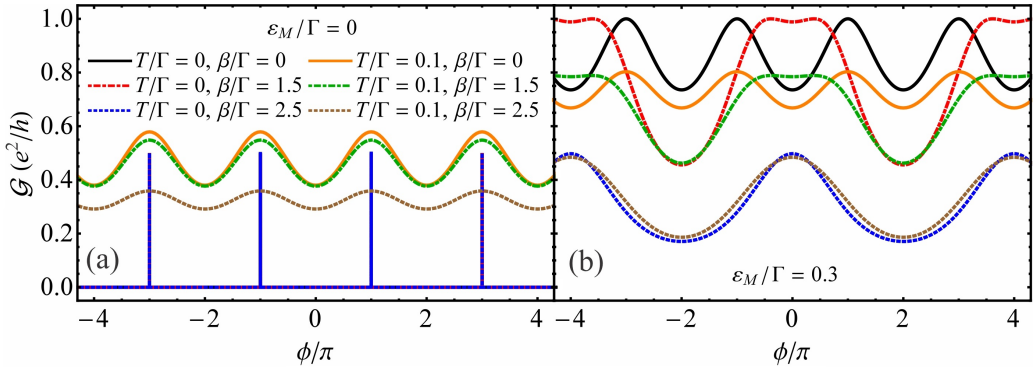

Figure 2.5: $\mathcal{G}$ versus ϕ for different values of β for: (a) $\varepsilon_M = 0\,\Gamma$ and (b) $\varepsilon_M = 0.3\,\Gamma$. The rest of parameters are: $|\lambda_1| = |\lambda_2| = 0.3\,\Gamma$ and $\varepsilon_d = 0\,\Gamma$.

ductance can be eliminated with a good approximation at $\tilde{\varepsilon}_d = 0$ when tuning the QD level to $\varepsilon_d = \beta^2/\omega_0$. In summary, when EPI is introduced, the periodicity of $\mathcal{G}$ as a function of ϕ switches between 2π and 4π values when changing $\tilde{\varepsilon}_d$ through the dot level ε_d or EPI strength β for hybridized MBSs.

In Figures 2.6(a) and (b) the differential conductance dI/dV versus magnetic flux phase ϕ is plotted at zero temperature for $\varepsilon_M = 0$ and $\varepsilon_M \neq 0$, with different β values at couplings $|\lambda_1| = |\lambda_2|$ and dot energy $\varepsilon_d = 0$ with a given value of the bias voltage eV. In the case of $\beta = 0$, dI/dV shows a 2π periodicity in magnetic flux phase ϕ for unhybridized MZMs. We observe that by varying β, a transition between 2π and π in the periodicity of dI/dV for nonoverlapping and between 2π and 4π for overlapping MBSs can be achieved. Figures 2.6(c) and (d) show the results for dI/dV versus ϕ at zero temperature, in the absence and presence of EPI, when the dot level is tuned $\varepsilon_d \neq 0$, for $\varepsilon_M = 0$ and $\varepsilon_M \neq 0$, with $|\lambda_1| = |\lambda_2|$ when β and eV are fixed. We can see that when the dot level meets $\varepsilon_d = \beta^2/\omega_0$, the renormalized QD energy vanishes $\tilde{\varepsilon}_d = 0$, resulting in the suppression of the EPI effect on the periodicity of dI/dV. Thus, the periodicity of differential conductance alters when tuning the QD level ε_d.

We hope that our findings clear up the expected behavior for MBS fingerprints in transport experiments where EPI plays a central role.

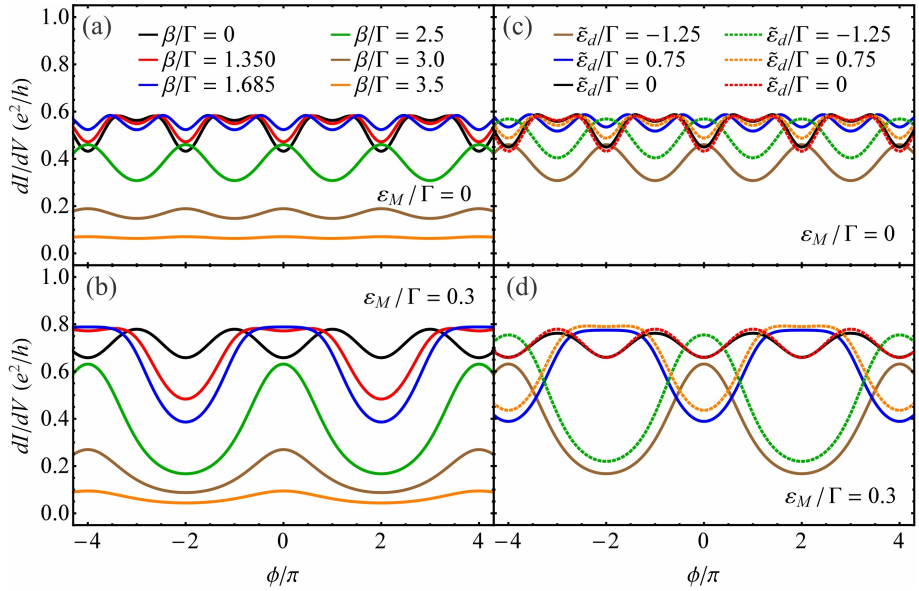

Figure 2.6: (a), (b) dI/dV versus ϕ for different values of β at $\varepsilon_d = 0\,\Gamma$ and (c), (d) dI/dV versus ϕ at different dot energies ε_d, with and without EPI ($\tilde{\varepsilon}_d = \varepsilon_d - \beta^2/\omega_0$), where the solid (dashed) lines correspond to $\beta = 2.5\,\Gamma$ ($\beta = 0\,\Gamma$) with $eV = 0.28\,\Gamma$, $|\lambda_1| = |\lambda_2| = 0.3\,\Gamma$ and $T = 0\,\Gamma$. The overlap energy is: (a), (c) $\varepsilon_M = 0\,\Gamma$ and (b), (d) $\varepsilon_M = 0.3\,\Gamma$.

Chapter 3

Nonequilibrium Kondo Physics of a Quantum Dot Connected to Graphene Leads in the Presence of Magnetic Fields

3.1 Motivation

The discovery of graphene [24] has extended the existing research areas and allowed the development of novel quantum nanodevices based on graphene [55] which reveal unique physical properties [22]. Such quantum devices are nanojunctions whose implementation can based on the coupling of quantum dots (QDs) to much larger systems like metallic [49, 50], ferromagnetic [56], or graphene leads [57–59]. The choice of electrodes can significantly influence the transport properties of the QD-based setup. The Kondo effect in QDs connected to normal leads has been extensively analyzed theoretically by using the Anderson impurity model within the equation of motion (EOM) framework [50, 60]. There have been many experimental efforts to confirm the Kondo effect in such systems [10, 61]. The effect of magnetic adatoms on physical properties of graphene has been theoretically investigated in the literature [62, 63]. Details on the experimental investigation of Kondo effect in graphene induced by lattice vacancies or magnetic adatoms via transport characteristics have been reported elsewhere [64, 65]. Up to now, a couple of theoretical works have been addressed in the literature to analyze thermoelectric characteristics of QDs connected to graphene systems [57–59].

The aim of this Chapter is to investigate the nonequilibrium Kondo-type transport in an QD with finite Coulomb energy attached to graphene leads for which the dot is threaded by a magnetic field.

3.2 Theoretical Model

We consider a QD coupled to two leads realized from monolayer graphene as it is illustrated

in Figure 3.1. The system is modeled by the Hamiltonian [57–59, 63]:

$$\begin{aligned}\mathcal{H} = &\sum_{\alpha,s,\sigma}\int_{-k_c}^{+k_c} dk\,\varepsilon_k\, c^{\dagger}_{\alpha sk\sigma}c_{\alpha sk\sigma} + \sum_{\sigma}\varepsilon_{d\sigma}d^{\dagger}_{\sigma}d_{\sigma} + Un_{d\uparrow}n_{d\downarrow}\\ &+\sum_{\alpha,s,\sigma}\int_{-k_c}^{+k_c} dk\big\{\mathcal{V}_{\alpha s\sigma}(k)c^{\dagger}_{\alpha sk\sigma}d_{\sigma} + [\mathcal{V}_{\alpha s\sigma}(k)]^{*}d^{\dagger}_{\sigma}c_{\alpha sk\sigma}\big\}.\end{aligned} \tag{3.1}$$

The first term in (3.1) models the massless Dirac fermions in the leads where $c^{\dagger}_{\alpha sk\sigma}(c_{\alpha sk\sigma})$ is the creation (annihilation) operator for massless Dirac fermions with momentum k and spin σ in the graphene lead α [$\alpha \equiv$ left (L) and right (R)]. In addition, s stands for the valley index and $\varepsilon_k = \hbar v_F k$ denotes the linear energy dispersion relation for massless Dirac fermions in graphene where the graphene Fermi velocity is v_F. The graphene leads are at the same temperatures, $T_\alpha = T$. We define a momentum cutoff k_c such that the linear dispersion relation to be fulfilled, where $D = \hbar v_F k_c$ being the energy cutoff. The second term in Eq. (3.1) describes the QD where $\varepsilon_{d\sigma} = \varepsilon_d + \sigma\Delta\varepsilon_d/2$ represents the spin-dependent QD energy level with $\sigma = +1$ for spin up ($\uparrow$) electrons and $\bar{\sigma} = -1$ for spin down ($\downarrow$) electrons. Here, $\Delta\varepsilon_d = |g|\mu_B B$ is the Zeeman splitting where g and μ_B are the Landé factor and the Bohr magneton, respectively. The notation $d_\sigma\,(d^{\dagger}_{\sigma})$ stands for the fermionic annihilation (creation) operator for an electron in the dot. The dot level can be tuned via the voltage applied to the gate electrode. The next term in Eq. (3.1) refers to the repulsion interaction of QD electrons with Coulomb energy U. Here, $n_{d\sigma} = d^{\dagger}_{\sigma}d_{\sigma}$ represents the occupation number operator for dot electrons with spin σ. The last term in relation (3.1) models the coupling of the localized electrons in QD to the graphene

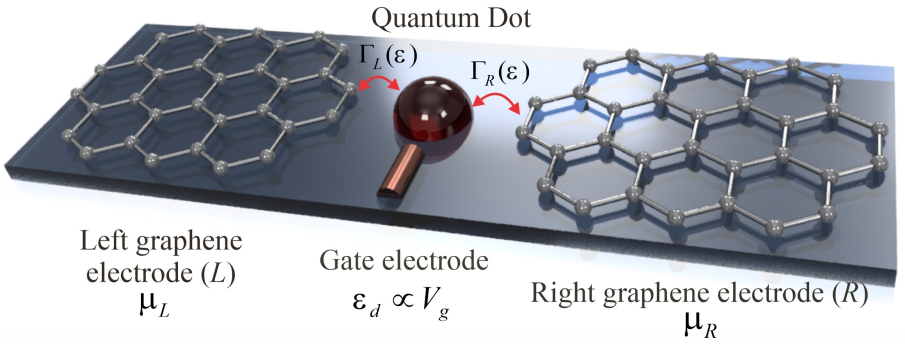

Figure 3.1: Schematic representation of a QD connected to left (L) and right (R) monolayer graphene leads with chemical potentials (μ_L and μ_R). Here, $\Gamma_\alpha(\varepsilon)$ stands for the coupling strength between the QD and α graphene lead. The spin-independent QD energy level ε_d is tuned by the gate voltage V_g via the gate electrode.

electrodes via tunneling amplitude $\mathcal{V}_{\alpha s\sigma}(k)$.

The total spin-dependent current flowing through the QD can be expressed as [49, 50]:

$$I_\sigma = \frac{e}{\hbar}\int_{-D}^{+D} d\varepsilon \frac{\Gamma_L(\varepsilon)\Gamma_R(\varepsilon)}{\Gamma_L(\varepsilon)+\Gamma_R(\varepsilon)}\big[f_L(\varepsilon)-f_R(\varepsilon)\big]\rho_{d\sigma}(\varepsilon), \tag{3.2}$$

where $\rho_{d\sigma}(\varepsilon) = -\mathrm{Im}G^r_{d\sigma}(\varepsilon)/\pi$ is the DOS of QD for electrons with spin σ, $G^r_{d\sigma}(\varepsilon)$ and $\Gamma_\alpha(\varepsilon) = 2\pi\eta|\varepsilon|\theta(D-|\varepsilon|)$ stand for the retarded Green's function of the QD and coupling strength between the dot and α graphene lead with η being a dimensionless coupling parameter. Here, $f_\alpha(\varepsilon)$ is the Fermi-Dirac distribution function for massless Dirac fermions in α graphene lead characterized by the μ_α chemical potential. The total DOS and total differential conductance are expressed as $\rho_d(\varepsilon) = \sum_\sigma \rho_{d\sigma}(\varepsilon)$ and $dI/dV = \sum_\sigma dI_\sigma/dV$, respectively. By knowing the retarded Green's function of the dot, all the transport properties of graphene-based QD device can be explored. To calculate $G^r_{d\sigma}(\varepsilon)$, we have used the EOM technique [53] combined with the broadly applied Lacroix's decoupling scheme [53]. The higher-order correlation functions appearing in the retarded Green's function have been determined within the framework of the Meir approximation [49]. The detailed computations regarding the retarded Green's function are presented in our article [66].

We found that the Kondo temperature vanishes at the Dirac point near the particle-hole symmetric point in the QD. In addition, away from the particle-hole symmetric point, the Kondo temperature remains finite even at the Dirac point which result is in agreement with numerical renormalization group calculations in the finite U limit [67]. Based on previous studies [68, 69], it can be established that the correct behavior of the Kondo temperature as a function of chemical potential is still not completely clarified even in the $U \to \infty$ limit for graphene-based systems. Additional analyses are needed to understand the behavior of Kondo temperature, also in the case of finite U. Note that a more correct estimation of the Kondo temperature needs self-consistent calculations rather then the non-self-consistent technique proposed by Meir et al. [49] and instead of using the Lacroix approximation [53], a more accurate decoupling scheme [60] is required.

3.3 Results and Discussion

In this Section, we present the main results performed for the QD-graphene nanodevice. To simplify the calculations, we used the energy cutoff D of graphene leads as the energy unit with $D \approx 7\,\text{eV}$ a reasonable value for graphene [59, 62]. The QD is realized from a GaAs heterostructure with system parameters presented in our paper [66].

We plot the DOS of QD for a finite Coulomb energy $U = 0.069\,D$ at three different values of the temperature T in the absence of magnetic field in Figure 3.2(a). We observe that the Kondo peaks emerge in the spectrum at the chemical potential of left ($\varepsilon \approx \mu_L$) and right ($\varepsilon \approx \mu_R$) leads. The Kondo resonances have a sharp lineshape at low temperatures and their magnitude decreases with the increase of temperature. At high temperatures, the Kondo peaks are totally washed out, in agreement with the results obtained previously for QDs connected to normal leads [50, 70]. In addition, beside the strongly temperature-dependent Kondo peaks, two broadened resonances show up in the DOS corresponding to resonant transmissions through the dot. Figure 3.2(b) illustrates the results of the total DOS with finite Coulomb energy $U = 0.069\,D$ at temperature $T = 5 \cdot 10^{-6}\,D$ in the presence of an external magnetic field. The magnetic field results in a splitting of Kondo peaks appearing initially at $\varepsilon = \mu_\alpha$ into two peaks with reduced amplitudes. The Kondo resonances are shifted by the Zeeman splitting from their nonmagnetic positions given by the chemical potentials to the higher energies for electrons with spin $\uparrow$ and to the lower energies for electrons with spin $\downarrow$. This behavior of the Kondo peaks is in agreement with the results of [50] for a QD coupled to normal leads in the presence of magnetic fields. It

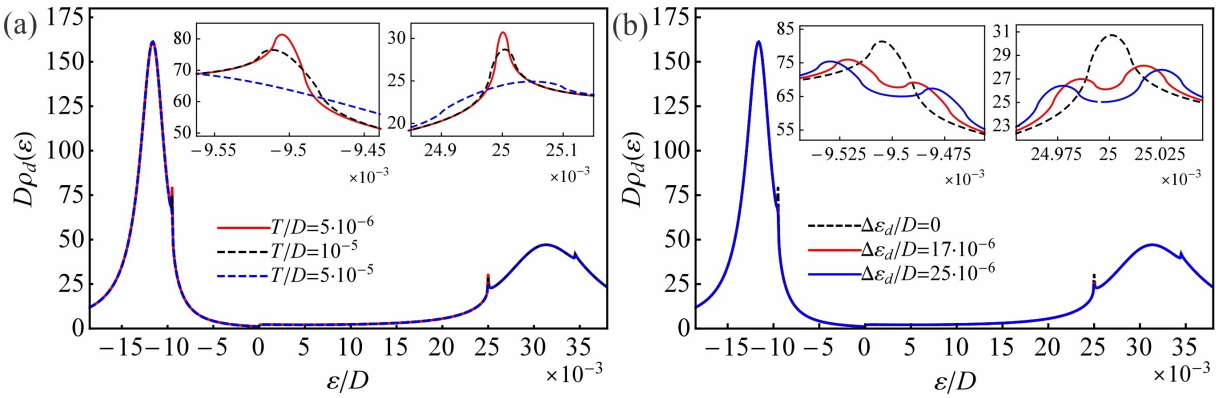

Figure 3.2: The nonequilibrium DOS of QD at different values of: (a) temperature T at $\Delta\varepsilon_d = 0\,D$ and (b) Zeeman splitting $\Delta\varepsilon_d$ at $T = 5 \cdot 10^{-6}\,D$ with $U = 0.069\,D$, $\mu_L = 25 \cdot 10^{-3}\,D$, $\mu_R = -9.5 \cdot 10^{-3}\,D$, $\eta = 0.02$ and $\varepsilon_d = -0.022\,D$.

is important to note that the DOS of QD vanishes at $\varepsilon = 0$ independently of the spin orientation. Furthermore, the Kondo resonances do not emerge in the DOS when the chemical potential in leads is pinned at the Dirac point, i.e., $\mu_\alpha = 0$, in agreement with the results obtained for an adatom placed on a graphene surface with $U \to \infty$ [71].

The numerical results for the differential conductance dI/dV through a strongly interacting QD ($U \to \infty$) as a function of applied bias voltage eV are shown in Figure 3.3(a) for different values of the temperature T in the absence of magnetic fields. The zero-bias peak develops in the differential conductance at low temperatures when the difference in chemical potentials matches the Zeeman splitting, i.e., $eV = \Delta\mu = \Delta\varepsilon_d = 0$, which represents a resonant transmission through the dot. The lineshape of Kondo peak strongly depends on temperature T and bias voltage eV. At low temperatures, the zero-bias peak has a sharper and narrow lineshape and with the grow in temperature, the amplitude of resonance reduces and broadens. The magnitude of the peak takes its maximum value at $eV = 0$ and it quickly drops when the bias voltage eV deviates from $eV = 0$. Figure 3.3(b) shows the numerical results for the differential conductance dI/dV against the bias voltage eV for different Zeeman splitting values $\Delta\varepsilon_d$ and at a fixed temperature value $T = 5 \cdot 10^{-6}\, D$. We observe that the applied magnetic field on QD leads to the splitting of zero-bias peak into two resonances with reduced amplitudes. Our results show a similar behavior with those systems composed from QDs connected to metallic electrodes threaded by magnetic fields [50].

We hope that the proposed QD-graphene system illustrated in Figure 3.1 will allow an experimental verification of our findings which can contribute significantly to the enlarging of the knowledge in graphene-based nanoelectronics.

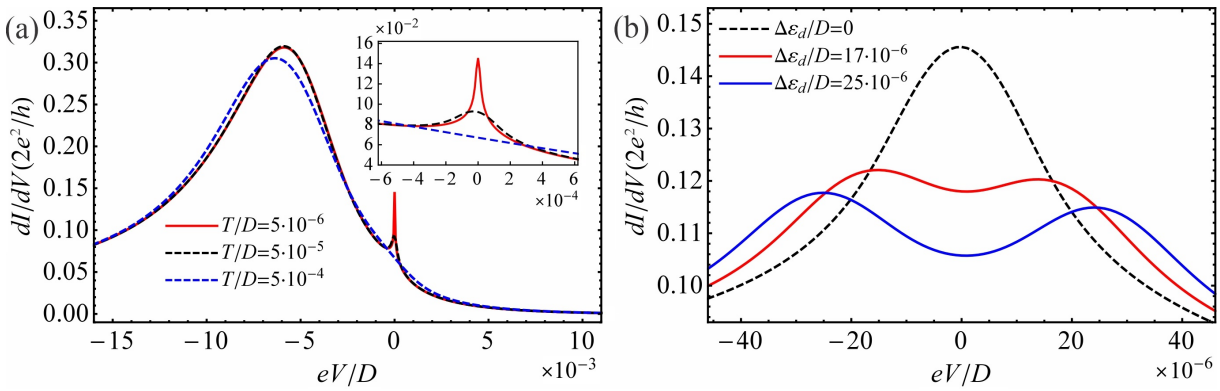

Figure 3.3: (a) dI/dV versus eV at different values of: (a) temperature T at $\Delta\varepsilon_d = 0\, D$ and (b) Zeeman splitting $\Delta\varepsilon_d$ at $T = 5 \cdot 10^{-6}\, D$ with $U \to \infty$, $\mu_R = -0.022\, D$, $\eta = 0.015$ and $\varepsilon_d = -0.068\, D$.

Chapter 4

Optical Properties of Spherical Quantum Dots: Application of the Inversely Quadratic Hellmann Potential

4.1 Motivation

The presence of quantum confinement in low-dimensional nanostructures could produce nonlinear optical effects, which are relevant in the development of optoelectronic devices, such as solar cells [72] and light-emitting diodes [73]. The theoretical studies in the literature indicate that the shape of spatial confinement potential for the motion of charge carriers in QDs plays an important role in the determination of optical properties of QDs [74–77]. The optical properties of low-dimensional semiconductor nanostructures such as quantum wells, quantum wires and QDs have been experimentally investigated in the literature [78–80].

The aim of this Chapter is to theoretically investigate the optical properties of a spherical QD in which the spatial confinement of charge carriers is modeled by the inversely quadratic Hellmann (IQH) potential. We discuss in detail the influence of the characteristic size of QD, confinement potential parameter and incident optical intensity on the absorption coefficient and on the refractive index changes in the case of a two-level QD system.

4.2 Theoretical Model

In our model, we approximate the spatial confinement for the motion of an electron in a spherically symmetric QD with an IQH potential, which, within Taylor series, is expressed as [81]:

$$V(r) \approx V_0 \left[\frac{1}{2} - 2\frac{R_0}{r} + \left(\frac{R_0}{r} \right)^2 \right], \tag{4.1}$$

where R_0 and V_0 are the characteristics size of QD and a potential parameter, respectively. Within the framework of effective-mass approximation, the time-independent Schrödinger equa-

tion of the system, in spherical coordinates, is separable into radial and orbital equation. The solutions of last one are given by the spherical harmonics, while, the radial equation has been solved by using the parametric Nikiforov-Uvarov method [82, 83].

Knowing the energy levels of the QD with the corresponding wavefunctions, the optical properties of the system can be analyzed. We have considered a two-level QD system irradiated by light and studied the behavior of optical absorption coefficient and relative changes in refractive index by varying R_0, V_0 and optical intensity I. The optical absorption coefficient $\alpha(\omega)$ is expressed a sum of first-order (linear) $\alpha^{(1)}(\omega)$ and third-order nonlinear $\alpha^{(3)}(\omega)$ optical absorption coefficients, $\alpha(\omega) \approx \alpha^{(1)}(\omega) + \alpha^{(3)}(\omega)$. Similarly, the relative changes in refractive index is a sum of first-order (linear) $\Delta n^{(1)}(\omega)/n_r$ and third-order nonlinear $\Delta n^{(3)}(\omega)/n_r$ terms, $\Delta n(\omega)/n_r = \Delta n^{(1)}(\omega)/n_r + \Delta n^{(3)}(\omega)/n_r$ [75].

4.3 Results and Discussion

In this Section, we present the main results on the optical properties of a QD realized from a GaAs heterostructure with system parameters presented in our paper [81].

We plot the linear $\alpha^{(1)}(\omega)$, third-order nonlinear $\alpha^{(3)}(\omega)$ and total $\alpha(\omega)$ absorption coefficients as a function of photon energy $\hbar\omega$ in Figure 4.1(a) when the dot characteristic size R_0 is varied and the potential parameter V_0 is fixed and in Figure 4.1(b) when V_0 is tuned and R_0 is fixed at a given optical intensity I. We observe that $\alpha^{(1)}(\omega)$ and $\alpha(\omega)$ reach maximum values while $\alpha^{(3)}$ presents a minimum at photon energy equals the energy difference between the two levels, $\hbar\omega = E_{21}$. The maximum of $\alpha^{(1)}(\omega)$ and $\alpha(\omega)$ as well as the minimum of $\alpha^{(3)}(\omega)$ are shifted to the lower energies when the QD characteristic size R_0 is increasing [Figure 4.1(a)]. In

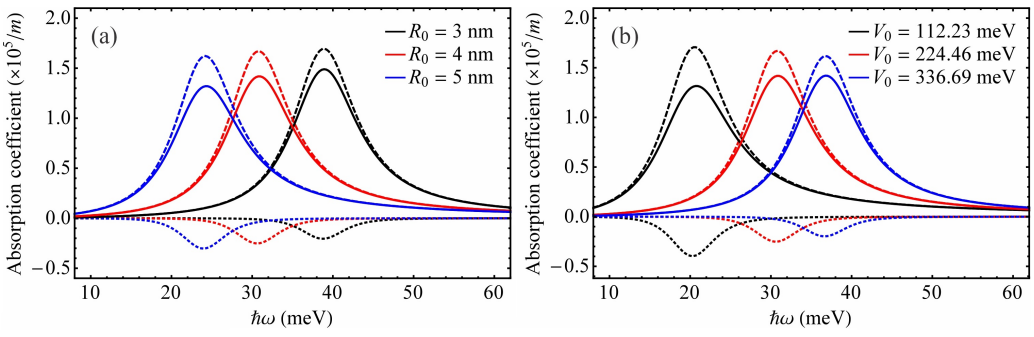

Figure 4.1: $\alpha^{(1)}(\omega)$ (dashed line), $\alpha^{(3)}(\omega)$ (dotted line) and $\alpha(\omega)$ (solid line) versus $\hbar\omega$ for different values of: (a) R_0 at $V_0 = 224.46$ meV and (b) V_0 at $R_0 = 4$ nm with $I = 8 \cdot 10^8$ W/m^2.

the case when V_0 is varied and R_0 is fixed, the position of $\alpha^{(1)}(\omega)$ and $\alpha(\omega)$ maxima, or the minimum of $\alpha^{(3)}(\omega)$ are shifted to the higher energy values with the increase of V_0 [Figure 4.1(b)].

We plot $\Delta n^{(1)}(\omega)/n_r$, $\Delta n^{(3)}(\omega)/n_r$ and $\Delta n(\omega)/n_r$ as a function of $\hbar\omega$ in Figure 4.2(a)-(c) when the QD characteristic size R_0 is varied at a constant V_0 and in Figure 4.2(d)-(f) when V_0 is varied at a given R_0 and optical intensity I. We see that $\Delta n^{(1)}(\omega)/n_r$, $\Delta n^{(3)}(\omega)/n_r$ and $\Delta n(\omega)/n_r$ intersect the zero value where the incident photon energy equals the energy difference between the levels, $\hbar\omega = E_{21}$. The position of intersection point shifts to lower energies with the increase of dot characteristic size R_0 at a fixed V_0 [Figure 4.2(a)-(c)]. When R_0 takes a constant value and the magnitude of V_0 is varied [Figure 4.2(d)-(f)], the intersection point of refractive index changes shift to higher energies with the increase of V_0.

We note that the increased incident optical intensity suppresses the amplitude of absorption coefficients and refractive index changes showing no effect on the position of their corresponding resonances or matching points.

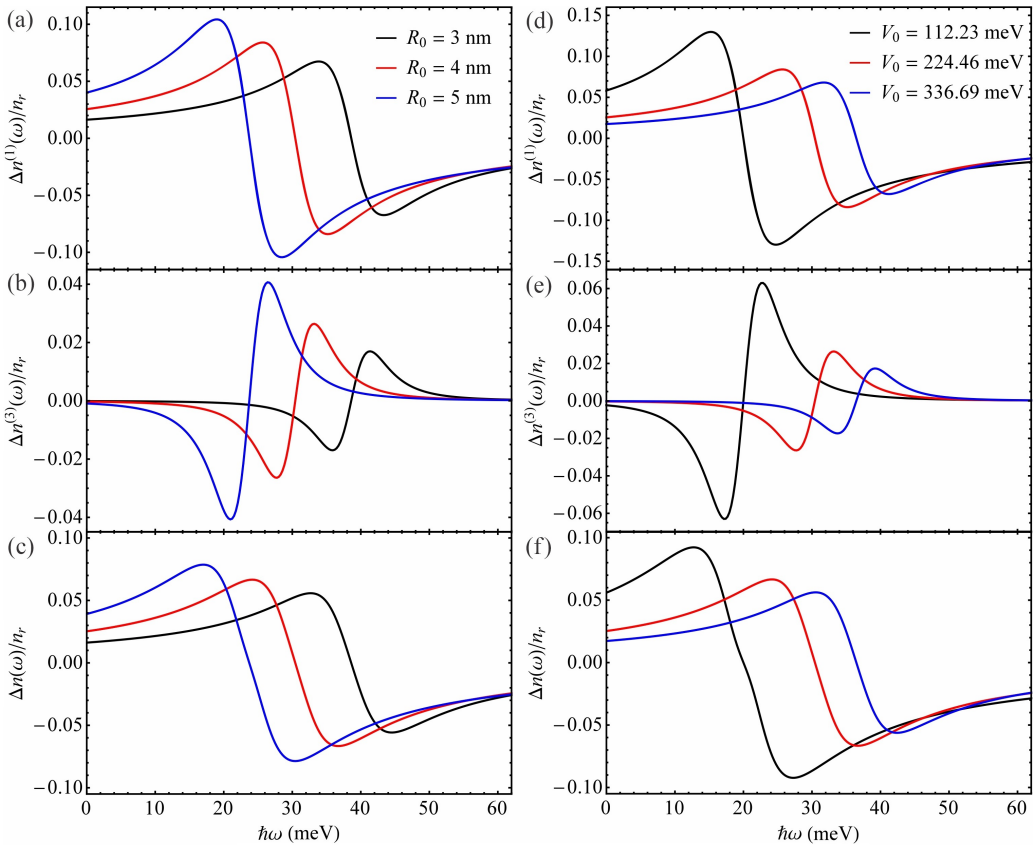

Figure 4.2: (a) $\Delta n^{(1)}(\omega)/n_r$, (b) $\Delta n^{(3)}(\omega)/n_r$, (c) $\Delta n(\omega)/n_r$ versus $\hbar\omega$ at different values of R_0 at $V_0 = 224.46\,meV$ and (d) $\Delta n^{(1)}(\omega)/n_r$, (e) $\Delta n^{(3)}(\omega)/n_r$, (f) $\Delta n(\omega)/n_r$ versus $\hbar\omega$ at different values of V_0 at $R_0 = 4\,nm$ with $I = 8 \cdot 10^8\ W/m^2$.

Conclusions and Outlook

The present thesis focuses on theoretical investigation of transport properties of different quantum dot (QD) nanodevices, based on topological superconducting nanowires (TSNW) or graphene. More precisely, we have studied the Majorana bound state (MBS) induced transport characteristics for a realistic QD system interacting with an optical phonon mode. The Kondo effect in an interacting QD attached to graphene leads has been investigated. In particular, the optical properties of spherical semiconductor QDs have been discussed where the spatial confinement is approximated with an inverse quadratic Hellmann (IQH) potential.

Chapter 1 of the thesis addresses a short discussion of quantum transport in low-dimensional systems such as QDs by presenting the Kondo effect. We have shortly reviewed the Majorana fermions, MBSs and the electronic properties of graphene. The last part of Chapter 1 of the thesis further describes the main phenomena characterizing the optical properties of two-level quantum systems realized in semiconductor QDs.

Chapter 2 of the thesis addresses theoretical study of transport properties of a Majorana circuit formed by two MBSs attached to a QD in the presence of electron-phonon interaction (EPI). The QD-MBSs ring structure is threaded by a tunable magnetic flux, which leads to manipulate the transport properties of the device. The interaction of the dot electron with an optical phonon mode results in phonon-assisted transport processes. The transport current flowing through the system has been determined using the nonequilibrium Green's function technique combined with a canonical transformation. We have found that the zero-temperature linear conductance exhibits a 2π periodicity in magnetic flux phase, and is immune to the presence of EPI, to changes in QD energy level, and finite values of dot-MZMs coupling for unhybridized Majoranas. The 2π periodicity of conductance transforms into 4π when the QD energy is nonzero or introducing EPI in the system for hybridized Majoranas. We have obtained that in the presence of EPI the periodicity of the differential conductance as a function of magnetic flux phase overgoes a transition from 2π to π for unhybridized Majoranas, and from 2π to 4π for overlapping MZMs, by changing the electron-phonon coupling strength. In particular, we have shown that the periodicity of differential and linear conductance remains unchanged also for an asymmetrically attached QD system in the absence of EPI which would facilitate the experimental

verification. The influence of EPI on transport current of a device where the QD connects only to one MBS has been also studied in detail. The device geometries discussed in this Chapter, should be experimentally feasible by taking into consideration the recent advances in nanotechnology [41, 42]. The results obtained here can hopefully serve as a guide for MBS-detection experimental measurements by using QDs. In the future, we would like to explore the transport properties of a more realistic device involving the coupling of a Majorana nanowire to a QD in the presence of EPI where the dot is asymmetrically connected to normal leads.

Chapter 3 of the thesis addresses a theoretical investigation of the nonequilibrium Kondo effect in a QD attached to two monolayer graphene leads when a magnetic field is applied to the QD. The retarded Green's function has been determined by using the equation of motion method within the Lacroix decoupling scheme [53] and Meir approximation [49]. We have deduced formulas for the Kondo temperature for different doppings of the graphene leads. The applied magnetic field leads to the splitting of the Kondo resonances that are destroyed at high temperatures. The zero-bias peak in differential conductance does not emerge when the leads' chemical potentials are pinned at the Dirac point. We hope that our findings can serve as a guide for the experimental verification of the Kondo effect in such QD-graphene systems proposed here by enlarging the knowledge in graphene-based nanoelectronics. In the future, we would like to determine the Green's function of the dot within a more precise decoupling scheme [60] beyond the Lacroix one [53] by employing self-consistent calculations instead of the Meir approximation [49]. The resulting Green's function can be a promising candidate to the analytical approximation of an improved formula for the Kondo temperature.

Chapter 4 of the thesis addresses a theoretical analysis of the linear and nonlinear optical properties of a two-level spherical QD realized in a GaAs semiconductor heterostructure. The spatial confinement for electrons has been approximated with an IQH potential. The eigensolutions of the radial Schrödinger equation have been found by applying the parametric Nikiforov-Uvarov method [82, 83]. We have found that the position of the resonances in the spectrum of optical absorption coefficients and the intersection point of refractive index changes can be shifted by varying the characteristic size of the dot or the potential parameter. We have obtained that the increasing light intensity suppresses the amplitude of absorption coefficients and refractive index changes. In the future, we plan to extend the investigation on the influence of external hydrostatic pressure and temperature on the optical properties of spherical QDs.

Selected Bibliography

[1] C. W. J. Beenakker, Phys. Rev. B **44**, 1646 (1991).

[2] D. Ryndyk, *Theory of Quantum Transport at Nanoscale: An Introduction* (Springer International Publishing, Cham, Switzerland, 2016).

[3] C. Fühner, *Magneto-transport investigations on multi-electron quantum dots: Coulomb blockade, Kondo effect, and Fano regime*, PhD dissertation, Hannover: Universität (2002).

[4] L. P. Kouwenhoven and P. L. McEuen, Single electron transport through a quantum dot, in *Nanotechnology*, edited by G. Timp (Springer New York, New York, NY, 1999) pp. 471–535.

[5] D. Goldhaber-Gordon, H. Shtrikman, D. Mahalu, D. Abusch-Magder, U. Meirav, and M. A. Kastner, Nature **391**, 156 (1998).

[6] L. Kouwenhoven and L. Glazman, Phys. World **14**, 33 (2001).

[7] R. Van Roermund, *Theoretical Study of non-equilibrium transport in Kondo quantum dots*, Theses, Université de Grenoble (2010).

[8] J. Kondo, Prog. Theor. Phys. **32**, 37 (1964).

[9] S. De Franceschi and W. van der Wiel, UndefinedKondo effect in quantum dots, in Undefined*Handbook of Nanophysics: Nanoparticles and Quantum Dots*, edited by K. Sattler (2010) pp. 646–664.

[10] S. M. Cronenwett, T. H. Oosterkamp, and L. P. Kouwenhoven, Science **281**, 540 (1998).

[11] J. Schmid, J. Weis, K. Eberl, and K. v. Klitzing, Physica B **256-258**, 182 (1998).

[12] E. Majorana, Nuovo Cim. **14**, 171 (1937).

[13] F. v. Oppen, Y. Peng, and F. Pientka, in *Topological Aspects of Condensed Matter Physics: Lecture Notes of the Les Houches Summer School: Volume 103, August 2014* (Oxford University Press, 2017).

[14] R. Aguado, Riv. Nuovo Cim. **40**, 523 (2017).

[15] V. Mourik, K. Zuo, S. M. Frolov, S. R. Plissard, E. P. A. M. Bakkers, and L. P. Kouwenhoven, Science **336**, 1003 (2012).

[16] A. Y. Kitaev, Phys. Usp. **44**, 131 (2001).

[17] Y. Oreg, G. Refael, and F. von Oppen, Phys. Rev. Lett. **105**, 177002 (2010).

[18] R. M. Lutchyn, J. D. Sau, and S. Das Sarma, Phys. Rev. Lett. **105**, 077001 (2010).

[19] P. Marra, J. Appl. Phys. **132**, 231101 (2022).

[20] R. Hützen, *Transport through interacting quantum dots with Majorana fermions or phonons*, PhD dissertation, Heinrich-Heine-University Düsseldorf (2013).

[21] J. Alicea, Rep. Prog. Phys. **75**, 076501 (2012).

[22] A. H. Castro Neto, F. Guinea, N. M. R. Peres, K. S. Novoselov, and A. K. Geim, Rev. Mod. Phys. **81**, 109 (2009).

[23] P. R. Wallace, Phys. Rev. **71**, 622 (1947).

[24] K. S. Novoselov, Science **306**, 666 (2004).

[25] R. Tarcan, O. Todor-Boer, I. Petrovai, C. Leordean, S. Astilean, and I. Botiz, J. Mater. Chem. C **8**, 1198 (2020).

[26] Q. He, S. Wu, Z. Yin, and H. Zhang, Chem. Sci. **3**, 1764 (2012).

[27] K. Rana, J. Singh, and J.-H. Ahn, J. Mater. Chem. C **2**, 2646 (2014).

[28] A. Olabi, M. A. Abdelkareem, T. Wilberforce, and E. T. Sayed, Renew. Sustain. Energy Rev. **135**, 110026 (2021).

[29] S. Das Sarma, S. Adam, E. H. Hwang, and E. Rossi, Rev. Mod. Phys. **83**, 407 (2011).

[30] J.-N. Fuchs and M. Goerbig, in *Introduction to the physical properties of graphene. Lecture notes* (2008).

[31] K. Flensberg, Phys. Rev. Lett. **106**, 090503 (2011).

[32] D. E. Liu and H. U. Baranger, Phys. Rev. B **84**, 201308 (2011).

[33] Y. Cao, P. Wang, G. Xiong, M. Gong, and X.-Q. Li, Phys. Rev. B **86**, 115311 (2012).

[34] J. P. Ramos-Andrade, P. A. Orellana, and S. E. Ulloa, J. Phys.: Condens. Matter. **30**, 045301 (2018).

[35] L. S. Ricco, Y. Marques, J. E. Sanches, I. A. Shelykh, and A. C. Seridonio, Phys. Rev. B **102**, 165104 (2020).

[36] M. Leijnse, New J. Phys. **16**, 015029 (2014).

[37] R. López, M. Lee, L. Serra, and J. S. Lim, Phys. Rev. B **89**, 205418 (2014).

[38] Q.-B. Zeng, S. Chen, L. You, and R. Lü, Front. Phys. **12**, 127302 (2016).

[39] A. M. Calle, M. Pacheco, P. A. Orellana, and J. A. Otálora, Ann. Phys. **532**, 1900409 (2020).

[40] A. D. K. Finck, D. J. Van Harlingen, P. K. Mohseni, K. Jung, and X. Li, Phys. Rev. Lett. **110**, 126406 (2013).

[41] M. T. Deng, S. Vaitiekenas, E. B. Hansen, J. Danon, M. Leijnse, K. Flensberg, J. Nygård, P. Krogstrup, and C. M. Marcus, Science **354**, 1557 (2016).

[42] M.-T. Deng, S. Vaitiekėnas, E. Prada, P. San-Jose, J. Nygård, P. Krogstrup, R. Aguado, and C. M. Marcus, Phys. Rev. B **98**, 085125 (2018).

[43] N. Dai and Q.-F. Sun, Phys. Rev. B **99**, 085436 (2019).

[44] X.-Q. Wang, B. Wu, S.-F. Zhang, Q. Wang, and W.-J. Gong, Ann. Physics **415**, 168127 (2020).

[45] X.-D. Wang, X.-Q. Wang, H.-Y. Sun, X.-F. Dai, Q. Wang, and W.-J. Gong, Phys. Scr. **96**, 015805 (2021).

[46] Z.-H. Wang, Front. Phys. (Lausanne) **9**, 704493 (2021).

[47] Z.-H. Wang and W.-C. Huang, Front. Phys. (Lausanne) **9**, 727934 (2021).

[48] Z.-Z. Chen, R. Lü, and B.-f. Zhu, Phys. Rev. B **71**, 165324 (2005).

[49] Y. Meir, N. S. Wingreen, and P. A. Lee, Phys. Rev. Lett. **66**, 3048 (1991).

[50] Y. Meir, N. S. Wingreen, and P. A. Lee, Phys. Rev. Lett. **70**, 2601 (1993).

[51] G. Michałek, B. R. Bułka, T. Domański, and K. I. Wysokiński, Phys. Rev. B **88**, 155425 (2013).

[52] J. Nilsson, A. R. Akhmerov, and C. W. J. Beenakker, Phys. Rev. Lett. **101**, 120403 (2008).

[53] C. Lacroix, J. Phys. F: Met. Phys. **11**, 2389 (1981).

[54] L. Máthé, D. Sticlet, and L. P. Zârbo, Phys. Rev. B **105**, 155409 (2022).

[55] H. Sun, L. Wu, W. Wei, and X. Qu, Mater. Today **16**, 433 (2013).

[56] J. Martinek, Y. Utsumi, H. Imamura, J. Barnaś, S. Maekawa, J. König, and G. Schön, Phys. Rev. Lett. **91**, 127203 (2003).

[57] T. Aono, J. Phys. Soc. Jpn. **82**, 083703 (2013).

[58] J. R. Isern-Lozano, J. S. Lim, I. Grosu, R. López, M. Crisan, and D. Sánchez, Eur. Phys. J. Spec. Top. **227**, 1969 (2019).

[59] S. Rodriguez, I. Grosu, M. Crisan, and I. Ţifrea, Physica E **96**, 1 (2018).

[60] R. Van Roermund, S.-y. Shiau, and M. Lavagna, Phys. Rev. B **81**, 165115 (2010).

[61] W. G. van der Wiel, S. D. Franceschi, T. Fujisawa, J. M. Elzerman, S. Tarucha, and L. P. Kouwenhoven, Science **289**, 2105 (2000).

[62] B. Uchoa, L. Yang, S.-W. Tsai, N. M. R. Peres, and A. H. Castro Neto, Phys. Rev. Lett. **103**, 206804 (2009).

[63] Z.-G. Zhu and J. Berakdar, Phys. Rev. B **84**, 165105 (2011).

[64] J.-H. Chen, L. Li, W. G. Cullen, E. D. Williams, and M. S. Fuhrer, Nat. Phys. **7**, 535 (2010).

[65] M. M. Ugeda, I. Brihuega, F. Guinea, and J. M. Gómez-Rodríguez, Phys. Rev. Lett. **104**, 096804 (2010).

[66] L. Máthé and I. Grosu, Beilstein J. Nanotechnol. **11**, 225 (2020).

[67] T. Kanao, H. Matsuura, and M. Ogata, J. Phys. Soc. Jpn. **81**, 063709 (2012).

[68] M. Vojta, L. Fritz, and R. Bulla, EPL **90**, 27006 (2010).

[69] T. Yanagisawa, J. Phys. Soc. Jpn. **84**, 074705 (2015).

[70] N. S. Wingreen and Y. Meir, Phys. Rev. B **49**, 11040 (1994).

[71] L. Li, Y.-Y. Ni, Y. Zhong, T.-F. Fang, and H.-G. Luo, New J. Phys. **15**, 053018 (2013).

[72] A. Nozik, Physica E **14**, 115 (2002).

[73] Z. Liu, C.-H. Lin, B.-R. Hyun, Z. Sher, Chin-Wei abd Lv, B. Luo, F. Jiang, T. Wu, C.-H. Ho, H.-C. Kuo, and J.-H. He, Light Sci. Appl. **9**, 83 (2020).

[74] W. Xie, Superlattices Microstruct. **46**, 693 (2009).

[75] W. Xie, Superlattices Microstruct. **48**, 239 (2010).

[76] A. Gharaati and R. Khordad, Superlattices Microstruct. **48**, 276 (2010).

[77] Y. Yakar, B. Çakır, and A. Özmen, Opt. Commun. **283**, 1795 (2010).

[78] M. Tanaka, H. Yamada, T. Maruyama, and K. Akimoto, Phys. Rev. B **67**, 045305 (2003).

[79] X.-L. Wang and V. Voliotis, J. Appl. Phys. **99**, 10.1063/1.2212056 (2006), 121301.

[80] H. An and J. Motohisa, Appl. Phys. Lett. **77**, 385 (2000).

[81] L. Máthé, C. Onyenegecha, A.-A. Farcaş, L.-M. Pioraş-Ţimbolmaş, M. Solaimani, and H. Hassanabadi, Phys. Lett. A **397**, 127262 (2021).

[82] A. F. Nikiforov and V. B. Uvarov, *Special Functions of Mathematical Physics* (Birkhauser Boston, 1988).

[83] C. Tezcan and R. Sever, Int. J. Theor. Phys. **48**, 337 (2009).

Dissemination of the Results

List of ISI Publications Related to the PhD Thesis

1. **L. Máthé**, Z. Kovács-Krausz, I. Botiz, I. Grosu, K. El Anouz, A. El Allati, and L. P. Zârbo*, "Phonon-assisted tunneling through quantum dot systems connected to Majorana bound states", *Nanomater.* ***13****, 1616 (2023)*, (DOI: 10.3390/nano13101616).
   IF: 5.719
   AIS: 0.737

2. **L. Máthé***, D. Sticlet and L. P. Zârbo, "Quantum transport through a quantum dot side-coupled to a Majorana bound state pair in the presence of electron-phonon interaction", *Phys. Rev. B* ***105****, 155409 (2022)*, (DOI: 10.1103/PhysRevB.105.155409).
   IF: 3.908
   AIS: 0.977

3. **L. Máthé***, C. P. Onyenegecha, A.-A. Farcaş, L.-M. Pioraş-Ţimbolmaş, M. Solaimani and H. Hassanabadi, "Linear and nonlinear optical properties in spherical quantum dots: Inversely quadratic Hellmann potential", *Phys. Lett. A* ***397****, 127262 (2021)*, (DOI: 10.1016/j.physleta.2021.127262).
   IF: 2.707
   AIS: 0.483

4. **L. Máthé*** and I. Grosu, "Nonequilibrium Kondo effect in a graphene-coupled quantum dot in the presence of a magnetic field", *Beilstein J. Nanotechnol.* ***11****, 225 (2020)*, (DOI: 10.3762/bjnano.11.17).
   IF: 3.649
   AIS: 0.617

Other ISI Publications

1. **L. Máthé** and I. Grosu*, "Transport Through a Quantum Dot with Electron-Phonon Interaction", *Mater. Today: Proc.* ***5****, 15878 (2018)*, (DOI: 10.1016/j.matpr.2018.06.058).
   IF: -
   AIS: -

Note: "*" indicates the corresponding author

Conference/Workshop/School Attending

Oral Presentations

1. **L. Máthé**, D. Sticlet, L. P. Zârbo, "Phonon-assisted transport in quantum dot-Majorana wire systems", exosup2022: School on Exotic Superconductivity, 13-25 June 2022, Cargèse, Corse, France (student talk)

2. **L. Máthé**, D. Sticlet, L. P. Zârbo, "Detecting Majorana bound states in hybrid quantum dot-topological superconducting nanowire devices", 2nd Global Webinar on Materials Science and Engineering, 27 November 2021, in Webinar.

3. **L. Máthé**, D. Sticlet, L. P. Zârbo, "Probing Majorana bound states in a quantum dot-topological superconducting nanowire ring system", 38th Global Nanotechnology Congress, 01-02 November 2021, in Webinar

4. **L. Máthé**, D. Sticlet, L. P. Zârbo, "Quantum transport through a quantum dot side-coupled to a Majorana bound state pair in presence of electron-phonon interaction", 13th International Conference on Physics of Advanced Materials (ICPAM-13), 24-30 September 2021, Sant Feliu de Guixols, Spain

5. **L. Máthé**, D. Sticlet, L. P. Zârbo, "Introduction to Majorana bound states: transport through a quantum dot coupled to Majorana bound states in presence of electron-phonon interaction", High Impedance Quantum Circuits, 6-10 August 2019, Villa Nante, Piedmont, Italy

6. **L. Máthé**, I. Grosu, "Thermoelectric transport through a quantum dot connected to graphene leads: Transition from the Coulomb blockade to the Kondo regime", 19th International Balkan Workshop on Applied Physics and Materials Science (IBWAP 2019), 16-19 July 2019, Constanţa, Romania

7. **L. Máthé**, I. Grosu, "Splitting of the Kondo peak in a quantum dot attached to graphene contacts", 24th International Conference on Chemistry, 24-27 October 2018, Sovata, Romania

Poster Presentations

1. **L. Máthé**, D. Sticlet, L. P. Zârbo, "Majorana induced phonon-assisted transport in asymmetrically coupled quantum dot nanodevices", International Conference on Quantum Communication, Measurement and Computing (QCMC 2022), 11-15 July 2022, Lisbon, Portugal.

2. **L. Máthé**, D. Sticlet, L. P. Zârbo, "Phonon-assisted transport in quantum dot-Majorana wire systems", exosup2022: School on Exotic Superconductivity, 13-25 June 2022, Cargèse, Corse, France.

3. **L. Máthé**, D. Sticlet, L. P. Zârbo, "Majorana bound state signatures in current through quantum dots in the presence of electron-phonon coupling", 38th Global Nanotechnology Congress, 01-02 November 2021, in Webinar

4. **L. Máthé**, D. Sticlet, L. P. Zârbo, "Quantum transport through a quantum dot coupled to a Majorana ring", 13th International Conference on Processes in Isotopes and Molecules (PIM 2021), 22-24 September 2021, Cluj-Napoca, Romania

5. **L. Máthé**, D. Sticlet, L. P. Zârbo, "Phonon-assisted transport in a quantum dot coupled to a Majorana bound state", VCQ Summer School 2021-Quantum Sensing & Imaging, 06-10 September 2021, Vienna, Austria

6. **L. Máthé**, D. Sticlet, L. P. Zârbo, "Andreev conductance through a quantum dot-Majorana ring structure", 4th Autumn School on Physics of Advanced Materials (PAMS 4), 24-30 September 2021, Sant Feliu de Guixols, Spain

7. **L. Máthé**, D. Sticlet, L. P. Zârbo, "Quantum transport through a quantum dot coupled to a Majorana ring in the presence of phonon modes", Workshop on Quantum Information Theory and Thermodynamics at the Nanoscale, 2-6 March 2020, Al-Hoceima, Morocco

8. **L. Máthé**, D. Sticlet, L. P. Zârbo, "Transport through a quantum dot coupled to Majorana bound states in presence of electron-phonon interaction ", Conference on Signatures of Topology in Condensed Matter, 21-25 October 2019, Trieste, Italy

9. **L. Máthé**, D. Sticlet, L. P. Zârbo, "Effect of the electron-phonon interaction on the transport properties of a quantum dot connected to Majorana bound states", 12th International Conference on Processes in Isotopes and Molecules (PIM 2019), 25-27 September 2019, Cluj-Napoca, Romania

10. **L. Máthé**, I. Grosu, "Graphene-based single electron transistor: transition from the Coulomb blockade to Kondo effect", Interfaces in Organic and Hybrid Thin-Film Optoelectronics (INFORM-19), 5-7 March 2019, Valencia, Spain

11. **L. Máthé**, I. Grosu, "Kondo Resonance splitting in a graphene-based quantum dot", 10th International Conference on Nanomaterials –R&A (NANOCON 2018), 17-19 October 2018, Brno, Czechia

12. **L. Máthé**, I. Grosu, "Nonequilibrium Kondo effect in a quantum dot coupled to graphene electrodes in presence of a magnetic field", 12th International Conference on Physics of Advanced Materials (ICPAM-12), 22-28 September 2018, Heraklion, Greece

13. **L. Máthé**, I. Grosu, "Transport through a strongly interacting quantum dot coupled to graphene electrodes", 3rd International Conference on Nanomaterials: Fundamentals and Applications (NFA 2017), 9-11 October 2017, Štrbské Pleso, Slovakia

School Attending

1. **L. Máthé**, School on Quantum Information Theory and Thermodynamics at the Nanoscale, 24-28 February 2020, Al-Hoceima, Morocco

Other Poster Presentations

1. **L. Máthé**, I. Grosu, "Transport through a quantum dot with electron-phonon interaction", 2nd Autumn School on Physics of Advanced Materials (PAMS-2), 8-14 September 2016, Cluj-Napoca, Romania

Awards

1. **L. Máthé**, D. Sticlet, L. P. Zârbo, "Andreev conductance through a quantum dot-Majorana ring structure", 4th Autumn School on Physics of Advanced Materials (PAMS 4), 24 30

September 2021, Sant Feliu de Guixols, Spain - **Sponsor's Prize** offered by American Elements

2. **L. Máthé**, I. Grosu, "Nonequilibrium Kondo effect in a quantum dot coupled to graphene electrodes in presence of a magnetic field", 12th International Conference on Physics of Advanced Materials (ICPAM 12), 22-28 September 2018, Heraklion, Greece - **Nicolae Sulitanu Prize** offered by Alina Sulitanu

Teaching Activity

1. 2016-2017 and 2017-2018: Teaching **Solid State Physics** seminars for 3rd year Physics Students at the Faculty of Physics, Babeș-Bolyai University

2. 2016-2017 and 2017-2018: Teaching **Electricity & Magnetism** seminars for 1st year Physics Students at the Faculty of Physics, Babeș-Bolyai University

Funding and Grants

1. PN-III-P1-1.2-PCCDI-2017-0338/79PCCDI/2018 (QUTECH-RO): "Developing Quantum Information and Quantum Technologies in Romania".

2. PN-III-P1-1.1-TE-2019-0423/TE98/08.09.2020: "Superconducting phases and quantum transport in two-dimensional transition metal dichalcogenides ".

3. MCID through the "Nucleu" Program within the National Plan for Research, Development and Innovation 2022–2027, project PN 23 24 01 04.

4. MCID through PNCDI III-Program 1-Development of the National Research and Development System, Subprogram 1.2-Institutional Performance-Funding Projects for Excellence in RDI, Contract No. 37PFE/30.12.2021.